CrossMark

ORIGINAL PAPER

Effect of High Temperature on Mineralogy, Microstructure, Shear Stiffness and Tensile Strength of Two Australian Mudstones

Xianfeng Liu[1] · Chonglei Zhang[1,2] · Shengyang Yuan[1] · Stephen Fityus[1] ·
Scott William Sloan[1] · Olivier Buzzi[1]

Abstract This study aims at providing quality experimental data on the effects of temperature on tensile strength and small strain shear stiffness of two Australian mudstones. The objective is to provide multiscale data in view of developing a numerical model that can capture and simulate the complex multiphysics of underground coal fire propagation. Two mudstones were collected in the Hunter Valley, close to a known underground coal fire, referred to as "Burning Mountain." The rock specimens were heated to a range of temperatures (maximum of 900 °C) for 24 h, and the materials were comprehensively characterized by X-ray diffraction, thermal gravimetric analyses, optical microscopy and scanning electron microscopy. In addition, mercury intrusion porosimetry was used in order to track changes in pore size distribution with temperature.

Investigations at microscale were complemented by testing at the macroscale. In particular, the paper focuses on the evolution of the tensile strength and small strain shear stiffness as the materials are subjected to heating treatment. Results show that both parameters evolve in a non-monotonic manner with temperature. The observed mechanical responses are fully explained and corroborated by microstructural observations.

✉ Olivier Buzzi
  Olivier.buzzi@newcastle.edu.au

  Xianfeng Liu
  Xianfeng.liu@newcastle.edu.au

  Chonglei Zhang
  chongleizhang2010@163.com

  Shengyang Yuan
  Shengyang.yuan@uon.edu.au

  Stephen Fityus
  Stephen.fityus@newcastle.edu.au

  Scott William Sloan
  scott.sloan@newcastle.edu.au

[1] Priority Research Centre for Geotechnical and Materials Modelling, ARC Centre of Excellence for Geotechnical Sciences and Engineering, The University of Newcastle, Callaghan, NSW 2308, Australia

[2] Key Laboratory of Mountain Hazards and Earth Surface Processes, Institute of Mountain Hazards and Environment, Chinese Academy of Sciences, Chengdu 610041, China

1 Introduction

A large number of coal-producing nations are confronted to an environment threat posed by underground coal fires (See Stracher and Taylor 2004). Such fires can be caused by human activities (e.g., mining) or triggered by natural causes (exothermic oxidation reaction followed by auto-combustion, bush fire, lightning). A number of studies reported in the literature showed that such fires are detrimental to mine safety, infrastructure and threaten the natural environment through their contribution to greenhouse gas emissions (CO_2 and CO) (Stracher and Taylor 2004; Sinha and Singh 2005; Kuenzer et al. 2007, to name few). Also, a large amount of valuable non-renewable resources are lost to these fires. An interesting feature of underground coal fires is their very slow burning kinetics. For example, "Burning Mountain," NSW, Australia, has been active for more than five thousands of years (Rattigan 1967). The burning kinetics is controlled by the oxygen availability (Stracher and Taylor 2004), which rarefies with depth. However, Ide et al. (2010), among others, have showed that the overburden strata often collapse as the coal burns and

cannot support the soil above it. Consequently, large cracks form under a combination of shear and tensile stress, and oxygen can access the fire again. Such mechanisms are illustrated in Fig. 1. Modeling the multiphysics propagation of underground coal fire hence requires an adequate modeling of the opening of cracks in the overburden mass and an adequate understanding of the effect of high temperatures on the mechanical response of the rocks lying above the burning coal seam.

So far, a number of studies have looked at the effect of temperature on the compressive strength and stiffness of natural rocks (mainly sandstones) (Dmitriev 1972; Somerton 1992; Tian et al. 2012, 2014; Zhang et al. 2009; Luo and Wang 2011; Ranjith et al. 2012; Brotóns et al. 2013, to name few), but there are still limited data on how high temperature might modify the tensile strength or shear stiffness of rocks. Such data are yet very important if one wants to model underground coal fire propagation (Liu et al. 2012) and investigate the options for fire extinguishment. Interestingly, it is only recently that a small number of researchers have tried to explain the macroscale observations by changes occurring at a microscale (e.g., Hajpál and Török 2004; Wolf 2006; Keshavarz et al. 2010; Yavuz et al. 2010). A preliminary study presented by the authors (Liu et al. 2016) focused on the temperature effects on compressive strength and permeability of two sedimentary rocks (a mudstone and a sandstone). Although the present study and that reported in Liu et al. (2016) are related in context, the present work focuses on different mechanical parameters and materials. This paper aims at providing quality and comprehensive data on the sensitivity to temperature of tensile strength and small strain shear stiffness of two Australian mudstones. The study also adopts a multiscale approach where comprehensive mineralogical and microstructural investigations are used to explain the macroscale response. Such comprehensive multiscale approach still remains marginal in the literature. The experimental program includes Brazilian test, shear wave velocity measurement, X-ray diffraction, thermal gravimetric analysis, optical microscopy, back-scattered scanning electron microscopy and mercury intrusion porosimetry. The outcomes of this work will provide quality data to allow modeling the propagation of an underground coal fire with possible tensile stress-induced failure of the overburden rock mass and formation of cracks.

2 Materials

Two sedimentary rocks were collected from a mine site of the Hunter Valley, New South Wales, Australia. The rocks were chosen because they are similar to those forming the overburden strata of Burning Mountain (Rattigan 1967). Figure 2 shows two specimens and some images obtained from transmitted light microscopy. The latter show that about 79.4 % (Fig. 2c) and 94.4 % (Fig. 2d) of the rock matrix contains particles smaller than 30 μm. According to the classification by Berkman (2001), this indicates that both rocks classify as mudstone. In the following, the rocks will be referred to as mudstones M1 and M2. The M1 material contains clear horizontal bedding planes (Fig. 2a) while M2 appears to be more homogenous (Fig. 2b). The optical microscopy analysis shows similar mineral components in the two rocks (mainly quartz, clay minerals, muscovite, feldspar, siderite). Note that dolomite was found in M2 (Fig. 2d) but not in M1 (Fig. 2c).

The specific gravity of both mudstones was measured using an automatic gas pycnometer (Micromeritics Autopyc II 1340, accuracy of 0.05 %), and the bulk density was determined following ASTM standard (ASTM-D4404-10 2010).

The main physical properties of these mudstones and their main mineralogical composition are summarized in Table 1.

Fig. 1 Sketch representing the opening of fractures in the overburden rock as it is progressively left unsupported
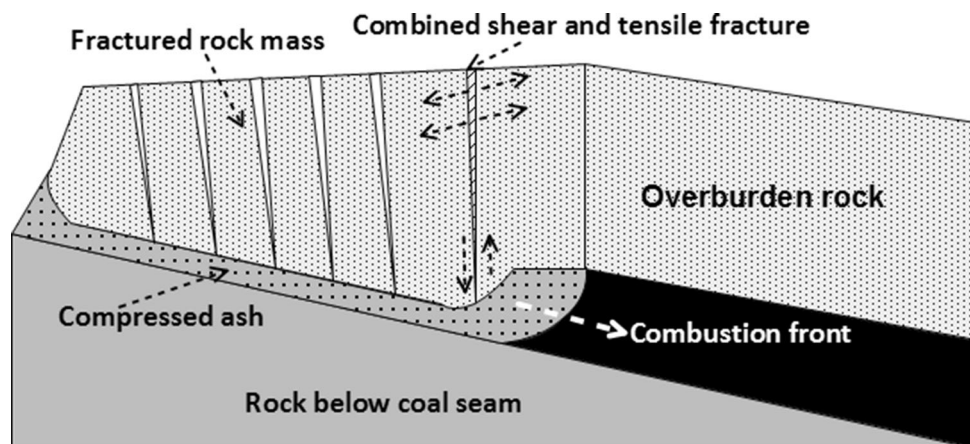
Fig. 2 View of the two specimens of mudstones tested and transmitted light microscopy images on thin sections: M1 (**a**, **c**) and M2 (**b**, **d**)

(a) Mudstone - M1

(b) Mudstone – M2

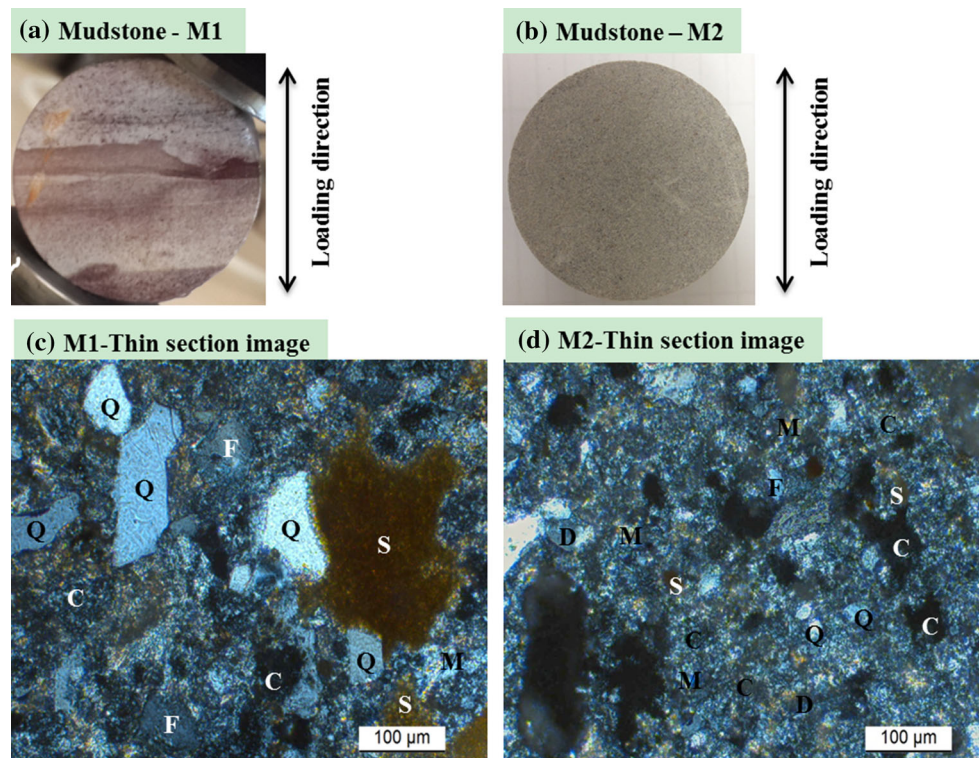(c) M1-Thin section image

(d) M2-Thin section image

Table 1 Physical properties and dominant mineral composition of mudstones tested

Rock type	Mineralogical composition from optical microscopy observation on thin sections	Specific gravity (G_s)	Bulk density (g/cm^3)	Initial porosity (n)
Mudstone (M1)	Clay minerals, quartz, siderite, muscovite, feldspar	2.71	2.40	0.11
Mudstone (M2)	Clay minerals, quartz, siderite, muscovite, feldspar, dolomite	2.68	2.38	0.11

3 Experimental program and methods

3.1 Experimental program

This experimental study aims at characterizing the changes occurring at macro- and microscales when the mudstones are exposed to temperatures up to 900 °C for 24 h. The effect of heating treatment was first assessed in terms of mineralogical changes within the rock specimens. This was achieved via a combination of semi-quantitative X-ray diffraction analysis (XRD) and optical microscopy observation on thin sections (OM). Note that the initial mineralogy was ascertained via thermal gravimetric analysis (TGA) on specimens heated to 100° in order to remove moisture. More microscale investigations were conducted to explain the changes observed at the macroscale. These included pore size distribution by mercury intrusion porosimetry (MIP), analysis of microstructural texture by back-scattering scanning (BES) electron microscopy and energy dispersive spectroscopy (EDS). Finally, the effect of heating on the mechanical properties was assessed via bender element tests

and Brazilian tests. Measuring the shear wave velocity of the material allows quantification of small strain stiffness and assessment of structural anisotropy.

The rocks were subjected to temperatures of 100 (reference condition), 300, 450, 600, 750 and 900°. For each temperature and each rock, 2 shear wave velocity tests, 2 Brazilian tests, 1 XRD and 1 MIP were conducted. In addition, each rock was subjected to 1 OM and 1 BES combined with EDS at 100, 600 and 900°.

3.2 Experimental Methods

3.2.1 Specimen Preparation and Heating Treatment

All rock specimens were cored in blocks retrieved from the mine site. The cored cylindrical specimens (diameter of 35.4 mm) were then cut a thickness of 20.2 mm, as recommended by ASTM-D4543-08 and ASTM-D3967-08. Note that the specimens for M1 were prepared with the bedding planes perpendicular to loading direction (vertical) as indicated in Fig. 4b.

All specimens were first dried at 100 °C for 24 h to remove the natural moisture. Then, a temperature-controlled furnace was used to reach target temperatures of 300, 450, 600, 750 and 900 °C. Heating was achieved at a rate of 1 °C/h, maintained for 24 h and followed by a cooling phase at 25 °C/h. Both the initial and final temperatures were set at 20 °C. After heating, the specimens were kept in a desiccator with desiccant gel in order to prevent any water uptake.

3.2.2 Shear Wave Velocity Measurement

Figure 3 presents the setup for shear wave velocity measurement. It consists of a metal base with two guiding columns and a moveable transverse beam. Two ultrasonic transducers (Panametrics-NDT/V152/10 MHz) are fixed on the base and the beam. Adequate and repeatable contact between transducers and rock specimens was achieved by placing a dead weight (2.5 kg) on the top beam. Input signals were generated and emitted using a programmable function generator (TTi®/40 MHz/DDS), and the signals were amplified (using a high voltage amplifier Pintek® HA-400) for a better accuracy. The frequency of the input signals varies from 10 to 50 kHz to ensure no influence of input signal on the shear wave velocity measurements and also facilitate the determination of the shear wave travel time. Output signals were also amplified with an ultrasonic preamplifier OLYMPUS® (Panametrics 5656C with a gain of 40 dB). Both input and output signals were recorded through a digital oscilloscope (Tektronix®, TDS, 1001C-EDU). The arrival time approach (first break pickup) proposed by Arroyo et al. (2010) was adopted to determine the travel time of the shear waves.

As shown in Fig. 3, the shear wave velocity measurements were conducted along the directions parallel and perpendicular to the loading direction.

The shear wave velocity (v_s) was used to infer the small strain shear modulus (G_0) of heated mudstones:

$$G_0 = \rho_b \cdot v_s^2 \tag{1}$$

where ρ_b is the bulk density of specimen (ASTM-D2845-08).

3.2.3 Brazilian Test

Brazilian tests were performed on the heated mudstone specimens having a thickness-to-diameter ratio of 0.57, which complies with ASTM standard D3967-08. The steel frame used for the shear wave measurement was also used to perform the Brazilian tests (see Fig. 4a). Two pieces of 3-mm-thick cardboard cushion were placed between the bearing plates and the specimen (Fig. 4b) to reduce stress concentration (as per ASTM standard D3967-08). Finally, a Geocom® compression system with a capacity of 70kN was employed to apply the load (at a rate of 0.45 mm/min).

3.2.4 Thermal Gravimetric Analysis (TGA)

Thermal gravimetric analyses were performed on powdered samples of rocks previously dried at 100° (particle size below 75 μm) in order to determine the mineralogy of the initial rock materials. The testing procedure and data interpretation method described in Pansu and Gautheyrou (2006) were followed. The tests were run under nitrogen environment while raising the temperature from 20 to 1100 °C at a rate of 5 °C/min. The mass loss and heat flow were recorded during the heating process, which allows the determination of the critical temperatures at which the dominant thermal reactions take place. This, in turn, permits the quantification of the dominant clay minerals.

3.2.5 Semi-Quantitative X-ray Diffraction Analysis (XRD)

X-ray diffraction analyses were conducted on powdered samples of heated rocks using a Philips X'Pert multipurpose diffractometer XRD with Cu K-alpha radiation (a

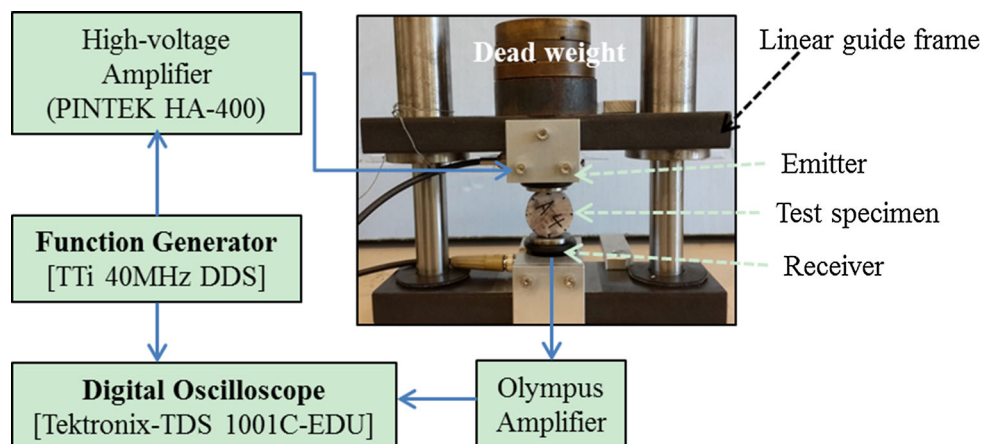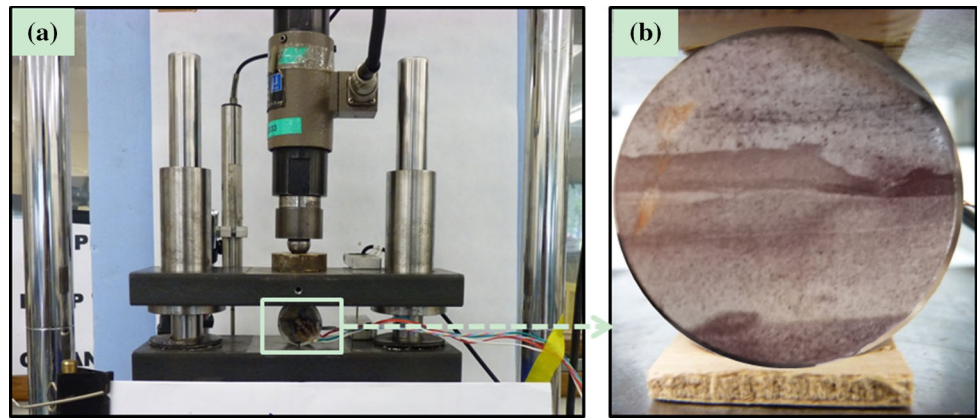**Fig. 3** Experimental setup for measuring shear wave velocity of mudstones tested

Fig. 4 Experimental setup for splitting test (**a**) and a typical specimen between two 3-mm-thick cardboard cushions (M1 heated at 600 °C) (**b**)

wavelength of 1.5406 Å), following the procedure described in Moore and Reynolds (1989). The diffraction pattern was recorded in 2θ steps of 0.007° during a continuous scan with a range of 2θ varying from 5.0° to 70°. Finally, the semi-quantitative analysis was performed on the XRD data by using a commercial package SIROQUANT based on ICDD-PDF2 database.
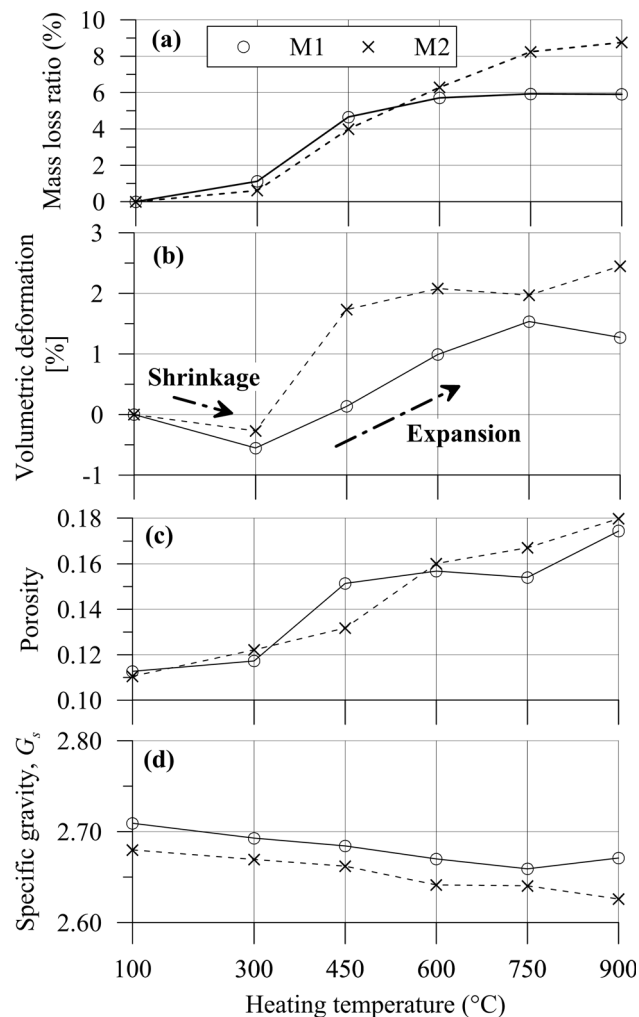
3.2.6 Optical Microscopy (OM) and Scanning Electron Microscopy (SEM) Observations

The changes in dominant minerals and related texture of mudstones induced by heating were further tracked by transmission and reflection light microscopy observations. These imaging techniques were performed on polished thin sections of specimens heated at 100, 600 and 900 °C. Back-scattering SEM (BS-SEM) and energy dispersive spectroscopy (EDS) were also applied to the thin sections to corroborate the conclusions drawn from the TGA and XRD analyses. A field emission microscope Zeiss Sigma VP FESEM was used and all the specimens were subjected to carbon coating prior to SEM observations.

3.2.7 Mercury Intrusion Porosimetry (MIP)

Pore size distributions were obtained using a Micromeritics AutoPore (IV 9500) with a capacity of 228 MPa, which corresponds to a minimum pore size of 6.5 nm. The apparatus tracks the volume of mercury intruding a specimen as the mercury pressure is incrementally increased. Intrusion and extrusion curves are produced as pressure is increased and decreased, respectively. The mercury injection pressure p is turned into an equivalent entrance pore size d using (as per ASTM-4404-10):

$$p = \frac{-4\sigma_{Hg}\cos\theta_{nw}}{d} \qquad (2)$$

where σ_{Hg} is the surface tension of mercury (0.484 N/m at 25 °C, as adopted by Diamond, 1970) and θ_{nw} is the mercury–mineral contact angle (assumed equal to 140° as per Romero, 1999). The specimens used for the MIP analysis have dimensions of 10 mm per 10 mm per 5 mm.

Fig. 5 Changes in mass loss ratio (**a**), volumetric deformation (**b**), porosity (**c**) and specific gravity (**d**) of mudstones when exposed to heating treatment. Positive volumetric deformation corresponds to expansion

Fig. 6 Evolution of shear wave velocity (**a**, **c**) and derived shear stiffness (**b**, **d**) with temperature along parallel (*vertical*) and perpendicular (*horizontal*) to loading direction. Each data point is an average of two measurements
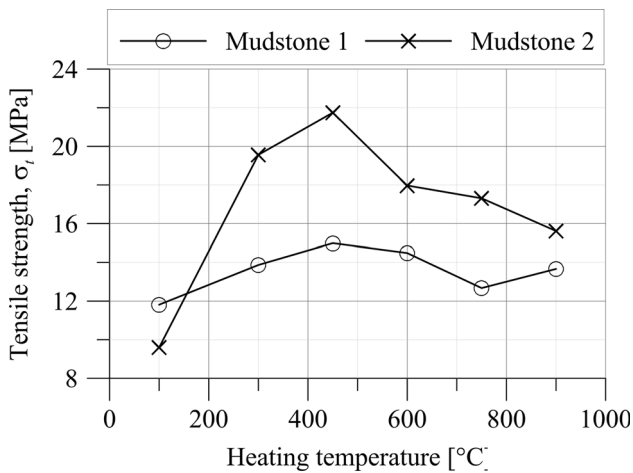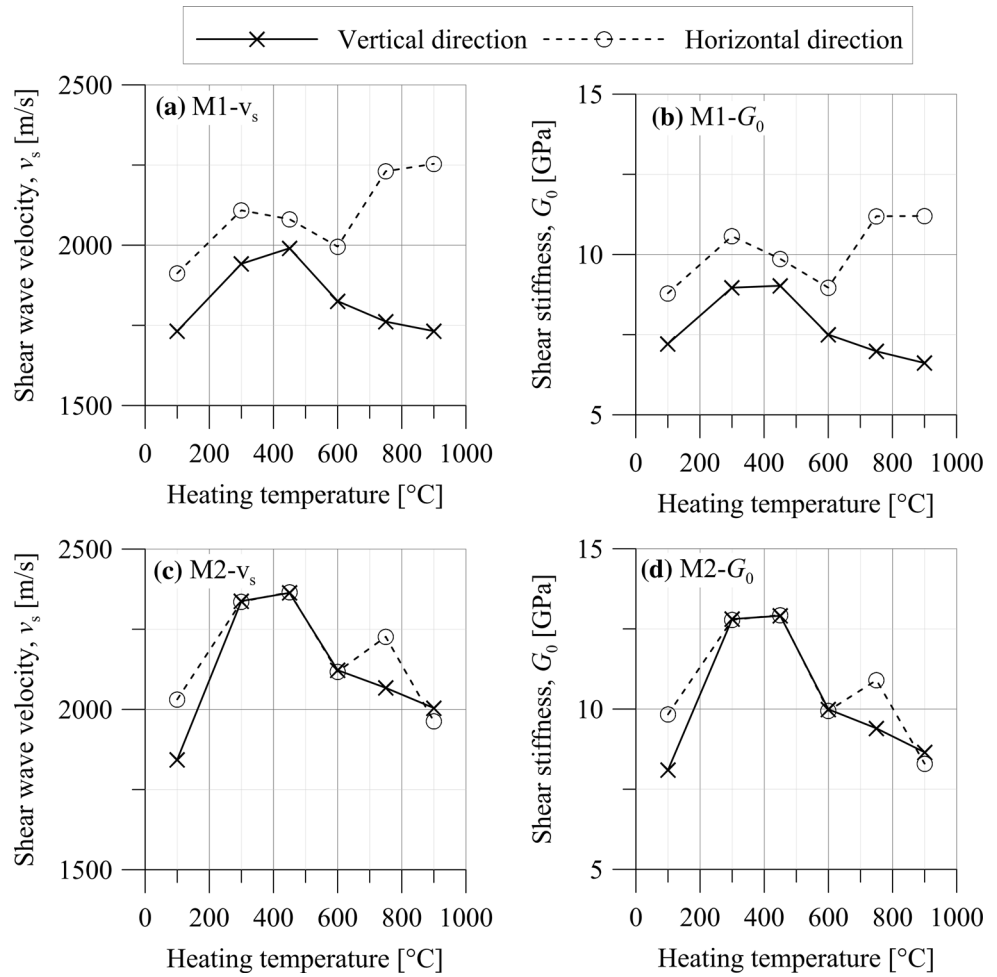

Fig. 7 Evolution of tensile strength with temperature. *Each data point* is an average of two measurements

Fig. 8 Thermal gravimetric analysis data expressed in terms of mass loss ratio (*continuous line*) and differential thermogravimetry (DTG, *dashed line*) for M1 (**a**) and M2 (**b**)

They were dried at 100 °C in order to remove moisture before MIP testing.

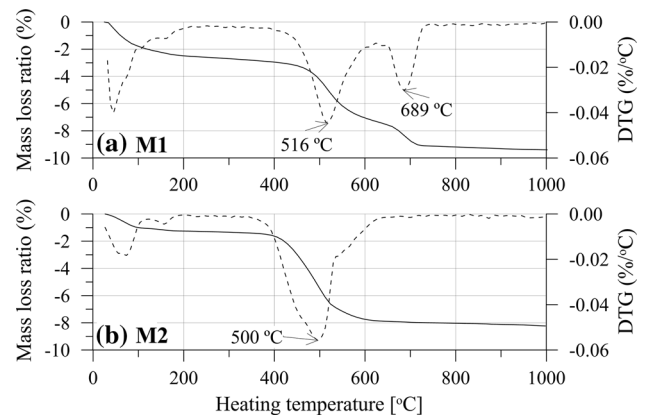In the rest of the paper, results will be discussed in terms of pore size density (PSD), which is the derivative of the cumulative intrusion curve, and in terms of intruded void ratio, which is defined as $e_{MIP} = V_{mercury}/V_{solids}$, where V_{solids} is the specimen volume and $V_{mercury}$ is the volume of intruded mercury at a given pressure.
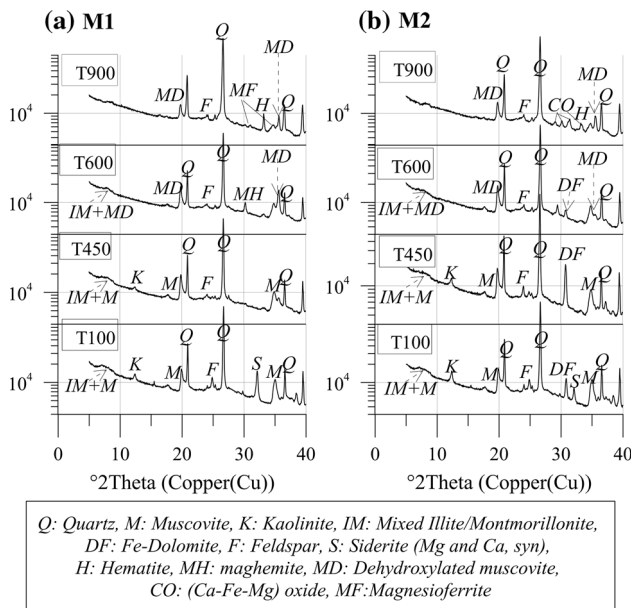
(a) M1 **(b) M2**

Q: Quartz, M: Muscovite, K: Kaolinite, IM: Mixed Illite/Montmorillonite,
DF: Fe-Dolomite, F: Feldspar, S: Siderite (Mg and Ca, syn),
H: Hematite, MH: maghemite, MD: Dehydroxylated muscovite,
CO: (Ca-Fe-Mg) oxide, MF:Magnesioferrite

Fig. 9 XRD results on mudstones subjected to heating treatment at 100, 450, 600 and 900 °C: M1 (**a**) and M2 (**b**)

4 Results and Discussion

4.1 Changes at Macroscale

4.1.1 Changes in Physical Parameters of Heated Rocks

Figure 5 presents the evolution of mass loss ratio, volumetric deformation, porosity and specific gravity with temperature. Both mudstones progressively and consistently lose mass as temperature rises (Fig. 4a). Interestingly, the specimens initially experience some shrinkage (<0.5 % for a temperature of 300 °C) before expanding. The expansion behavior is consistent with the observations by Somerton (1992) who reported a general increase in rock volume due to thermal expansion at high temperatures. The combined effects of the mass loss and volume change result in a consistent increase in porosity. Finally, a slight drop can be seen for the specific gravity of both mudstones in response to heating treatment. This can be attributed to the thermal reactions of dominant mineral compositions including muscovite, clay minerals and siderite for both rocks as well as dolomite only for M2. These thermal reactions will be further evidenced in the upcoming sections.

4.1.2 Changes in Shear Wave Velocity and Derived Shear Stiffness

Figure 6 shows the evolution of shear wave velocity (v_s) with temperature and the corresponding low-strain shear stiffness (G_0) values (calculated using Eq. 1) along the directions parallel and perpendicular to the loading direction (referred as vertical and horizontal direction, respectively). A clear structural anisotropy can be observed for M1 with higher shear stiffness along the horizontal direction (i.e., parallel to bedding planes, Fig. 6b), whereas no considerable anisotropy appears for M2 with similar shear stiffness along both vertical and horizontal directions (Fig. 6d). Furthermore, the pattern along the vertical direction is similar for both rock types: the stiffness initially augments (for temperatures up to 450 °C) before dropping back close to the initial value. With respect to M1, M2 clearly exhibits a higher stiffness along the vertical direction, which will later be explained by the mineralogical composition of the rocks.

4.1.3 Changes in Tensile Strength

Similar to the evolution of the shear stiffness, it is here found that the tensile strength evolves in a non-monotonic manner with temperature. Furthermore, the peak temperature is 450° and M2 exhibits the highest tensile strength (Fig. 7), as per Fig. 6. These observations will be explained by the complementary microstructural investigations to be presented in a later section.

4.2 Changes at Microscale

4.2.1 Changes in Mineralogy of Heated Rocks

Before investigating the changes in mineralogy, thermogravimetric analyses (TGA) were performed on both mudstones prior to any heating treatment in order to determine the initial mineralogy. Results are showed in Fig. 8.

The TGA patterns show that both mudstones experience a small mass loss below 100 °C, which results in a differential thermogravimetric (DTG) peak and can be explained by the removal of some free water.

Beyond 100 °C, mass is lost in a two stage process for M1 but in a single stage for M2. Indeed, two distinct peaks are visible at 516 and 689 °C for M1 while the sole TG peak of M2 occurs at 500 °C. This mass loss corresponds to the loss of structural water of clay minerals, muscovite and carbonates present in both mudstones (as evidenced by Dmitriev 1972; Somerton 1992). Such reaction is also called dehydroxylation (Pansu and Gautheyrou 2006).

Further interpretation of the TGA data, as per Pansu and Gautheyrou (2006), suggests that the dominant clay mineral in M1 is likely to be montmorillonite while M2 is kaolinite dominant. These results will be confirmed by the XRD analysis presented below.

Fig. 10 Transmitted (**a**, **c**) and reflected (**b**, **d**) light microscopy analysis on thin sections of mudstone (M1) subjected to heating at temperatures of 600 °C (**a**, **b**) and 900 °C (**c**, **d**)
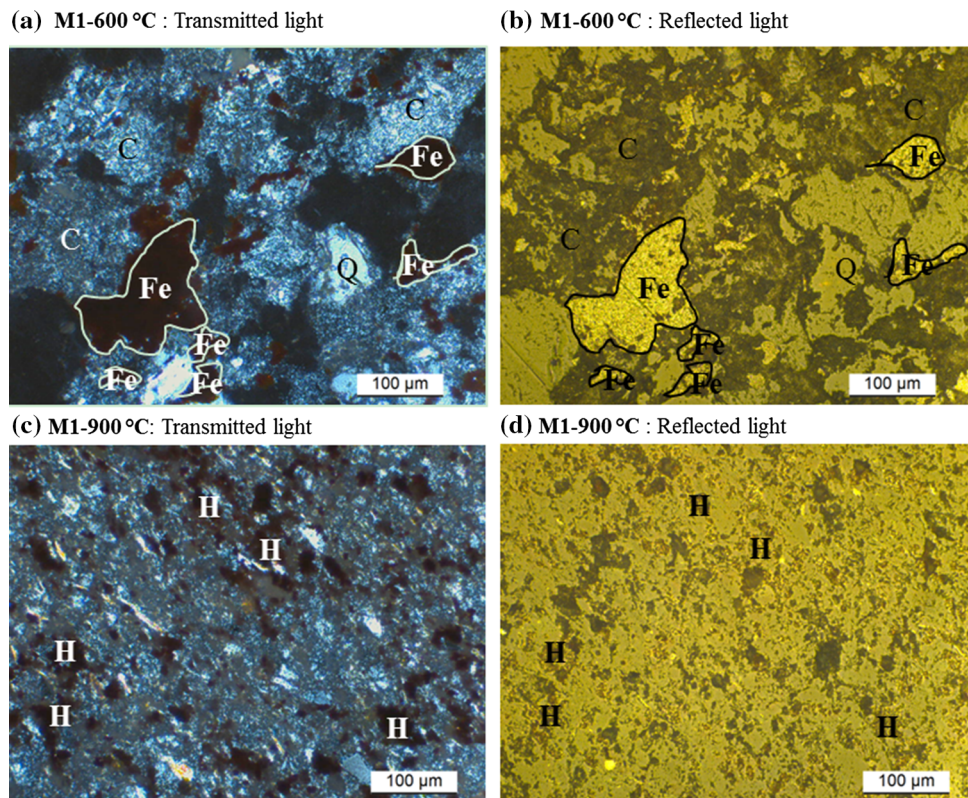

(a) **M1-600 °C** : Transmitted light

(b) **M1-600 °C** : Reflected light

(c) **M1-900 °C**: Transmitted light

(d) **M1-900 °C** : Reflected light

Fig. 11 Transmitted (**a**, **c**) and reflected (**b**, **d**) light microscopy analysis on thin sections of mudstone (M2) subjected to heating at temperature of 600 °C (**a**, **b**) and 900 °C (**c**, **d**)

(a) **M2-600 °C** : Transmitted light

(b) **M2-600 °C** : Reflected light

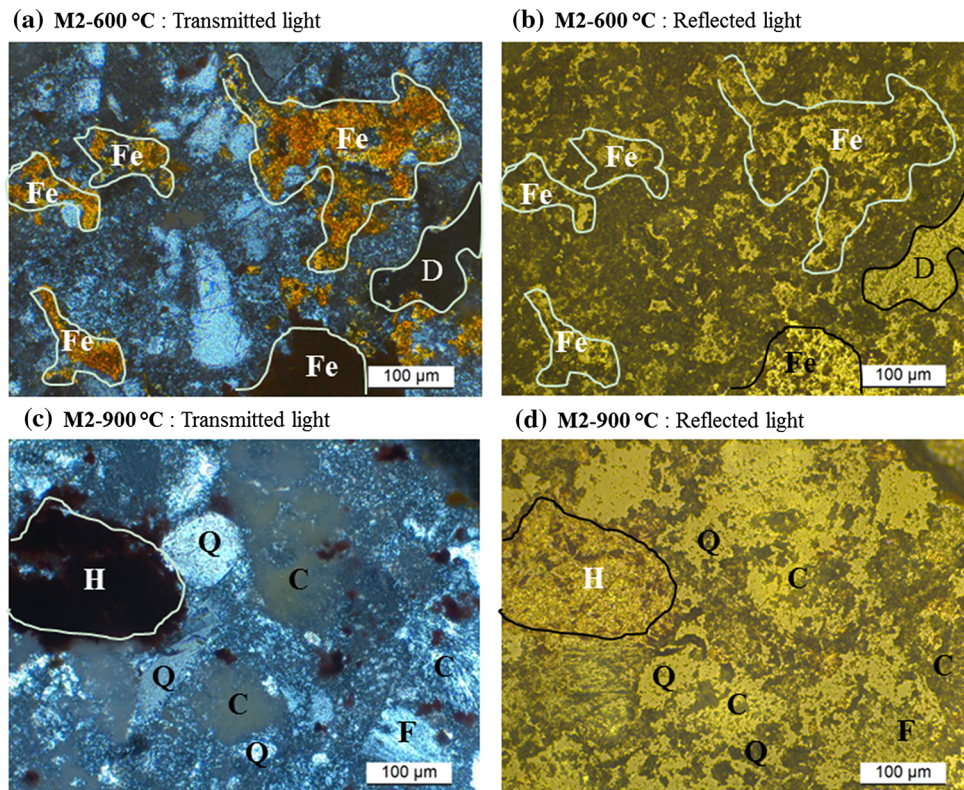(c) **M2-900 °C** : Transmitted light

(d) **M2-900 °C** : Reflected light

Table 2 Semi-quantitative XRD analysis on mudstones M1 and M2

Rock type	Minerals	Maximum temperature for heating treatment (°C)					
		100	300	450	600	750	900
Mudstone M1	Quartz	D	D	D	D	D	D
	Mixed illite/montmorillonite	SD	SD	SD	SD	A	–
	Muscovite	A	A	A	–	–	–
	Kaolinite	A	A	A	–	–	–
	Siderite (Mg and Ca, syn)	A	A	–	–	–	–
	Feldspar	Tr	Tr	Tr	Tr	Tr	Tr
	Dehydroxylated muscovite	–	–	–	A	A	A
	Fe-bearing oxides (Mg and Ca)	–	–	A	A	A	–
	Hematite	–	–	–	–	Tr	A
	Maghemite	–	–	–	Tr	–	–
	Magnesioferrite	–	–	–	–	Tr	A
Mudstone M2	Quartz	D	D	D	D	D	D
	Kaolinite	SD	SD	SD	–	–	–
	Siderite (Mg and Ca, syn)	A	A	–	–	–	–
	Fe–dolomite	A	A	A	A	A	–
	Mixed illite/montmorillonite	A	A	A	A	Tr	–
	Muscovite	A	A	A	–	–	–
	Feldspar	Tr	Tr	Tr	Tr	Tr	Tr
	Zirconium dioxide	Tr	Tr	Tr	Tr	Tr	Tr
	Dehydroxylated muscovite	–	–	–	A	A	A
	(Ca, Fe, Mg) oxides	–	–	A	A	A	A
	Hematite	–	–	–	–	A	A

D: Dominant. Used for the component apparently most abundant, regardless of its probable percentage level

SD: Subdominant. The next most abundant component(s) providing its percentage level is judged above about 20

A: Accessory. Components judged to be present between the levels of roughly 5 and 20 %

Tr: Trace. Components judged to be below about 5 %

Following the TGA on intact mudstones, XRD analyses were conducted on specimens following the heating treatment in order to track the changes in mineralogy with heating treatment. Note that, in order to enhance the clarity of the XRD pattern, only the range of 2θ below 40°, which includes all the relevant modifications, is presented.

Figure 9 shows that the dominant peaks are quite similar for both rock types. In particular, the following minerals are found in both materials: quartz, muscovite, feldspar, kaolinite, mixed illite/montmorillonite and siderite (Ca and Mg). In contrast, the Fe-bearing dolomite and Zirconium dioxide can be only identified in M2. Further semi-quantitative analysis confirms the outcomes of the TGA: The subdominant mineral in M1 is mixed Illite/Montmorillonite while it is kaolinite in M2. The XRD patterns in Fig. 8 suggest that quartz and feldspar do not undergo any significant modification for the range of temperature tested. This is essentially due to the fact that higher temperature is required to affect these minerals (Somerton 1992; Pansu and Gautheyrou 2006).

In contrast, a number of minerals do undergo changes. From temperature of 450 and up 650 °C, muscovite is progressively transformed into its dehydroxylated form (Somerton 1992). The interpretation of XRD data clearly shows that some minerals also tend to disappear upon heating. These are kaolinite and siderite (disappearing from 600 °C), mixed illite/montmorillonite (disappearing from 900 °C) and Fe–dolomite (disappearing from 750 °C). All these observations are quite consistent with the response of TGA (where the corresponding peaks progressively vanish).

Finally, some minerals form as a result of heating. For instance, Fe-bearing oxides (Ca and Mg) can clearly be identified in both mudstones heated at 600 °C (see Fig. 9) and hematite appears in both mudstones heated at 900 °C. Those newly formed minerals are also observed on the transmitted and reflected light microscopy conducted on polished thin sections (Figs. 10, 11). The appearance of the Fe-bearing oxides and the hematite can be attributed to the decomposition of Fe-bearing carbonates such as siderite for

Fig. 12 MIP results of heated M1 (**a**, **c**) and M2 (**b**, **d**) in terms of total mercury intrusion void ratio (**a**, **b**) and pore size distribution (**c**, **d**)
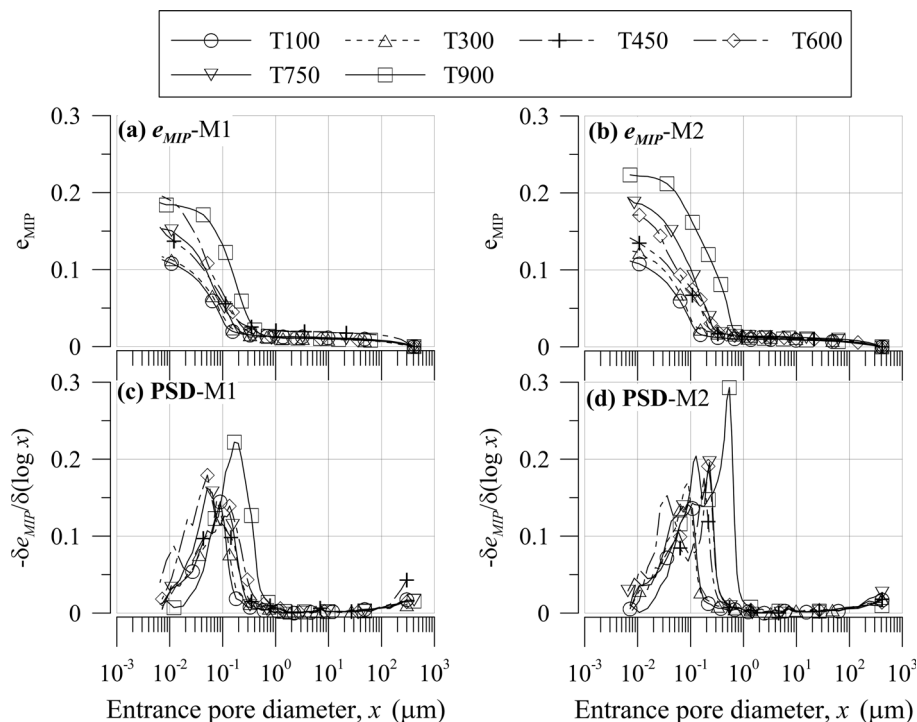
M1 and both siderite and Fe–dolomite for M2 (Hajpál and Török 1998, 2004).

The semi-quantitative mineralogical analysis based on the XRD patterns in Fig. 8 is summarized in Table 2.

4.2.2 Changes in Microstructure Inferred by MIP and SEM

This section will show that exposure to high temperature also affects the size and frequency of pores in both rocks. The MIP results on M1 and M2 are expressed in terms of intruded void ratio (Fig. 12a, b) and pore size distribution (Fig. 13c, d) for all temperatures tested.

For M1, the intruded void ratio (e_{MIP}) almost doubles (from 0.1 to 0.18) when the temperatures rises from 100 to 900 °C (Fig. 12a). This is accompanied by a progressive increase in pore volume density for a class pore size below 1.0 μm without affecting much the dominant pore size when the heating temperatures are below 750 °C (see Fig. 12c). It takes a rise in temperature to 900 °C to observe a significant increase in both dominant pore size and its density.

The evolution of the pore size distribution of M2 is more gradual with an increase in (e_{MIP}) for each step of temperature rise (Fig. 12b, d). As a result, both the dominant pore size and density augment when the temperature is raised up to 900 °C.

The changes observed in Fig. 12 can be explained by the generation of microcracks either by differential thermal expansion of the minerals or by the thermal reactions of the dominant minerals as discussed in the previous section.

The occurrence of such microcracks is confirmed by the back-scattering SEM images of the rocks heated at 100, 600 and 900 °C. These images include the dominant minerals determined by combining the XRD data (Fig. 9; Table 2) and the chemical analysis obtained by EDS (Fig. 12). Both mudstones initially have a dense micro-fabric (Fig. 13a, b), and the boundaries between the different minerals are quite clear. However, these boundaries are more difficult to draw under temperatures of 600 and 900 °C. The cementation minerals (e.g., Fe-bearing carbonates such as siderite and dolomite) are oxidized when exposed to high temperatures (600 and 900 °C) under oxygen environment (Deer et al. 2013). In addition, dehydroxylated clay minerals can be clearly detected at heating temperature of 600° (Fig. 13c, d). Finally, microcracks are clearly visible on both materials heated to 900 °C (Fig. 13e, f), particularly within the dehydroxylated clay minerals (Fig. 13f). These observations corroborate the conclusions drawn from the MIP analyses.

5 Conclusions

This study investigates the thermal effect on tensile strength of two Australian mudstones collected in a Hunter Valley Mine that is located close to an existing underground coal seam fire (Burning Mountain). The first part of

Fig. 13 Back-scattering SEM images on the thin sections of M1 (**a, c, e**) and M2 (**b, d, f**) subjected to heating at 100 °C (**a, b**), 600 °C (**c, d**) and 900 °C (**e, f**)
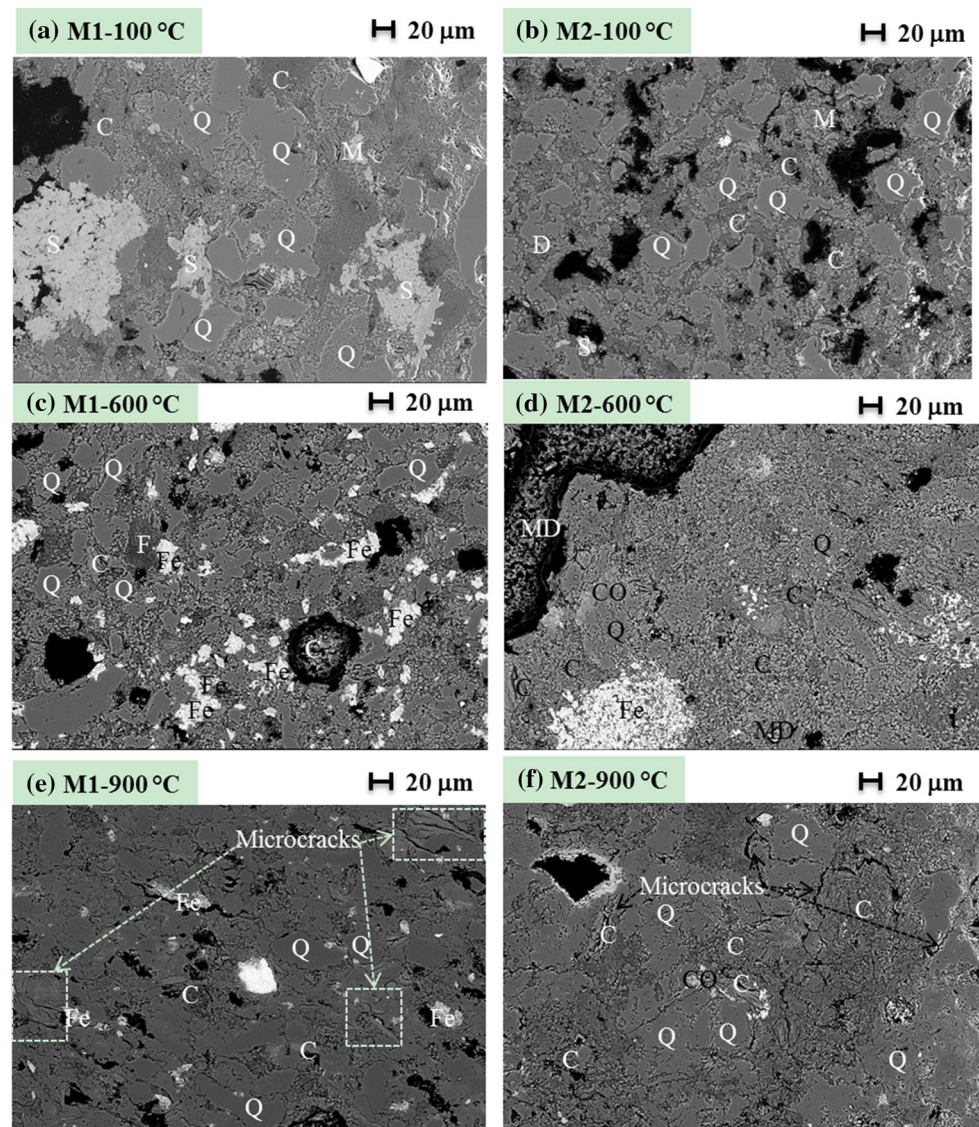
the paper presents the experimental evolution of low-strain shear stiffness and tensile strength with temperature. The macroscale testing was followed by a comprehensive analysis at microscale to explain the effects of the heating treatment on the behavior of the rocks from a multiscale approach. The main outcomes of this study can be summarized as follows:

1. For temperatures ranging from 100 to 450 °C, the dominant thermal reaction evidenced by XRD and TGA data is the dehydration of adsorbed water within the clay minerals contained in both mudstones, which is accompanied by the decomposition of (Mg, Ca) siderite. These reactions result in a significant loss of mass and a small decrease in their specific gravity. On the other hand, the differential thermal expansion of dominant minerals generates some microcracks, a phenomenon clearly evidenced by mercury intrusion porosimetry. The combination of thermal expansion, crack generation and mass loss yields an overall augmentation of porosity. On the other hand, it has been showed that cementation reaction is concurrently occurring upon heating, which prevails over the above-mentioned weakening effect in the 100–450 °C temperature range. The consequence of such microscale modifications is a significant augmentation of both tensile strength and low-strain shear stiffness.

2. A subsequent increase in heating temperatures from 450 up to 900 °C leads to the dehydroxylation reaction (loss of structural water) of clay minerals and in particular, of the muscovite contained in the mudstones. For M2, the dehydroxylation reaction is also accompanied by a progressive decomposition of Fe–dolomite. In this temperature range, the microcracks continue to develop (evidenced by a gradual shift of

dominant pore size) to become the predominant phenomenon. Consequently, both tensile strength and small strain shear stiffness are observed to decrease.

References

Arroyo M, Pineda JA, Romero E (2010) Shear wave measurements using bender elements in argillaceous rocks. Geotech Test J 33:1–11. doi:10.1520/GTJ102872

ASTM-D2845-08 (2008) Standard test method for laboratory determination of pulse velocities and ultrasonic elastic constants of rock. ASTM Int, West Conshohocken. doi:10.1520/D2845-08.2

ASTM-D3967-08 (2008) Standard test method for splitting tensile strength of intact rock core specimens. ASTM Int, West Conshohocken. doi:10.1520/D3967-08

ASTM-D4404-10 (2010) Standard test method for determination of pore volume and pore volume distribution of soil and rock by mercury intrusion porosimetry. ASTM Int, West Conshohocken. doi:10.1520/D4404-10

ASTM-D4543-08 (2008) Standard practices for preparing rock core as cylindrical test specimens and verifying conformance to dimensional and shape tolerances. ASTM Int, West Conshohock. doi:10.1520/D4543-08

Berkman DA (2001) Field geologist's manual, 4th edn. Australasian Institute of Mining and Metallurgy, Carlton

Brotóns V, Tomás R, Ivorra S, Alarcón JC (2013) Temperature influence on the physical and mechanical properties of a porous rock: San Julian's calcarenite. Eng Geol 167:117–127

Deer WA, Howie RA, Zussman J (2013) An introduction to the rock-forming minerals, 3rd edn. Mineralogical Society, London

Dmitriev A (1972) Physical properties of rocks at high temperatures. Folia Microbiol (Praha) 17:117–125. doi:10.1007/BF02877909

Hajpál M, Török A (2004) Mineralogical and colour changes of quartz sandstones by heat. Environ Geol. doi:10.1007/s00254-004-1034-z

Hajpál M, Török Á (1998) Petrophysical and mineralogical studies of burnt sandstones. In: Proceedings of 2nd international PhD symposium 1–9

Ide TS, Pollard D, Orr FM (2010) Fissure formation and subsurface subsidence in a coalbed fire. Int J Rock Mech Min Sci 47:81–93. doi:10.1016/j.ijrmms.2009.05.007

Keshavarz M, Pellet F, Loret B (2010) Damage and changes in mechanical properties of a gabbro thermally loaded up to 1,000 °C. Pure appl Geophys 167:1511–1523. doi:10.1007/s00024-010-0130-0

Kuenzer C, Zhang J, Tetzlaff A et al (2007) Uncontrolled coal fires and their environmental impacts: investigating two arid mining regions in. Appl Geogr 27:42–62. doi:10.1016/j.apgeog.2006.09.007

Liu XF, Collin F, Buzzi O, Sloan SW (2012) Numerical modelling of ground temperature evolution as a result of underground coal fire. Aust Geomech J 47:27–32

Liu XF, Yuan SH, Sieffert Y, Fityus S, Buzzi OP (2016) Changes in mineralogy, microstructure, compressive strength and intrinsic permeability of two sedimentary rocks subjected to high-temperature heating. Rock Mech Rock Eng. doi:10.1007/s00603-016-0950-z

Luo J, Wang L (2011) High-temperature mechanical properties of mudstone in the process of underground coal gasification. Rock Mech Rock Eng. doi:10.1007/s00603-011-0168-z

Moore MD, Reynolds RC (1989) X-ray diffraction and the identification and analysis of clay minerals. Oxford University Press, Oxford

Pansu M, Gautheyrou J (2006) Handbook of soil analysis: mineralogical, organic and inorganic methods. Springer, Berlin

Ranjith PG, Viete DR, Chen BJ, Perera MSA (2012) Transformation plasticity and the effect of temperature on the mechanical behaviour of Hawkesbury sandstone at atmospheric pressure. Eng Geol 151:120–127. doi:10.1016/j.enggeo.2012.09.007

Rattigan JH (1967) Phenomena about burning mountain, Wingen, New South Wales. Aust J Sci 30:183–184

Sinha A, Singh VK (2005) Spontaneous Coal seam fires: a global phenomenon. In: ERSEC Ecological Book Series-4 on Coal Fire Research. Beijing, PR China, pp 42–66

Somerton W (1992) Thermal properties and temperature-related behavior of rock/fluid systems. Elsevier, Amsterdam, The Netherlands

Stracher GB, Taylor TP (2004) Coal fires burning out of control around the world: thermodynamic recipe for environmental catastrophe. Combustion 59:7–17. doi:10.1016/j.coal.2003.03.002

Tian H, Kempka T, Xu N, Ziegler M (2012) Physical properties of sandstones after high temperature treatment. Rock Mech Rock. doi:10.1007/s00603-012-0228-z

Tian H, Ziegler M, Kempka T (2014) Physical and mechanical behavior of claystone exposed to temperatures up to 1000 °C. Int J Rock Mech Min Sci 70:144–153. doi:10.1016/j.ijrmms.2014.04.014

Wolf K-HAA (2006) The interaction between underground coal fires and their roof rocks. Delft University of Technology, TU Delft

Yavuz H, Demirdag S, Caran S (2010) Thermal effect on the physical properties of carbonate rocks. Int J Rock Mech Min Sci 47:94–103. doi:10.1016/j.ijrmms.2009.09.014

Zhang L, Mao X, Lu A (2009) Experimental study on the mechanical properties of rocks at high temperature. Sci China Ser E Technol Sci 52:641–646. doi:10.1007/s11431-009-0063-y